

ES Energy & Environment

DOI: https://dx.doi.org/10.30919/esee999



Design of Selective Metasurface Filter for Thermophotovoltaic Energy Conversion

Rajagopalan Ramesh,^{1, 2,*} Qing Ni,^{1, 3} Hassan Alshehri,^{1, 4} Bruno Azeredo² and Liping Wang^{1,*}

Abstract

Optical filters with narrow transmission band above the bandgap of thermophotovoltaic (TPV) cells are not restrained by the rigorous thermal reliability as needed for the emitters. In this work, a novel metasurface filter made of an aluminum nanopillar (AINP) array on a quartz substrate is proposed to achieve spectrally selective transmission above the bandgap of the TPV cell. Optical simulations using Finite-difference time-domain were carefully performed to determine the appropriate AINP period, diameter, and height such that the resulting nanopillar array will show narrowband transmission at a wavelength of 1.9 µm, which is close to the bandgap of a commercial gallium antimonide (GaSb) TPV cell. The narrow-band transmission enhancement can be attributed to the magnetic polariton (MP) resonance between neighboring Al nanopillars. The MP mechanism is further confirmed by an inductor-capacitor circuit model and the effects of the nanopillars' period, diameter, height, as well as incidence angles were discussed. Moreover, open-circuit voltage, short-circuit current density, output electric power, and conversion efficiency were evaluated for the GaSb TPV cell coupled with the AINP metasurface filter structure with enhanced TPV performance.

Keywords: Metasurface; Thermophotovoltaic; Optical filter, Nanopillars; Selective transmission.

Received: 11 August 2023; Revised: 23 October 2023; Accepted: 25 October 2023.

Article type: Research article.

1. Introduction

effect to convert thermal infrared radiation from an emitter into electricity. The TPV system is composed of a thermal emitter, a selective filter, and a photovoltaic cell.[1] The temperature for the emitter ranges between 1000 and 2000 K which is usually optimal for a cell with a bandgap range of 0.5-0.75 eV.[1,2] TPV energy conversion system allows recycling of waste heat and improves the thermal to electricity conversion efficiency.[3-6] Potential use of TPV systems includes nuclear power generation for space applications,[7] hybrid electric vehicles,[8] industrial and home power supplies, [9] waste heat recovery, [10] solar photovoltaic systems,[11] and portable electric generators.[12]

The maximum theoretical efficiency of a TPV system is A thermophotovoltaic (TPV) device uses the photovoltaic constrained by the radiative limit, [2,13] but practical TPV systems suffer from low output power generation and poor conversion efficiency partly due to the radiation spectrum mismatch between the thermal radiation spectrum of the emitter and absorption spectrum of the cell. In 2014, Fraas et al.[14] projected a TPV planar module performance for steel industry application at 1400 and 1500 K blackbody temperature with 20% efficiency and output power of 1.8 W/cm². Subsequently, a cell efficiency of 29% with an electric power of 1.5 W/cm² for a single GaSb cell measured under 1548 K glowing steel radiator temperature was reported.[14] Tan et al.[15] compared the performance of In_{0.53}Ga_{0.47}As and In_{0.68}Ga_{0.32}As and demonstrated that the cells obtained an efficiency of 16.4% and 19.1% at 1323 K blackbody temperature, respectively. Recent demonstrations show TPV cell efficiency ≥30% using two different cell materials, GaAs and InGaAs at emitter temperatures surpassing 1500 K.[16] The highest experimental conversion efficiency of more than 40% has been achieved with TPV systems consisting of twojunction cells made of III-V materials with bandgaps between 1.0 and 1.4 eV.[17] The cells exploited the edge-spectral filtering using highly reflective back surface reflectors to reject sub-bandgap radiation and were optimized for emitter

¹ School for Engineering of Matter, Transport & Energy, Arizona State University, Tempe, AZ 85287, USA.

² The Polytechnic School, Arizona State University, Mesa, AZ 85212, USA.

³ University of Science and Technology of China, Anhui 230052, China.

⁴ King Saud University, Riyadh 11451, Saudi Arabia.

^{*}Email: rrames14@asu.edu (R. Ramesh), Liping.Wang@asu.edu (L. Wang)

temperatures of 1,900-2,400°C.

To further improve the TPV performance, research has been done on designing selective emitters and optical filters. Broadband and selective emitters are the two most common types of emitters used in TPV applications. Broadband emitters follow Planck's law^[18] and emit photons across a broad range of wavelengths whereas selective emitters are designed to emit photons within a certain wavelength range. Bendelela *et al.*^[19] presented a TPV system with a metamaterial acting as the selective emitter. For a blackbody temperature of 1500 and 300 °C, a combination of InAs/GaInAsSb TPV tandem cell yielded theoretical conversion efficiencies of 41% and 11.82%, respectively. While recent advancements have focused on achieving

While recent advancements have focused on achieving spectrally selective thermal emitters using materials such as photonic crystals, [20] metamaterials, and multilayers, [21] it is worth noting that these materials can serve a dual purpose. They not only function as potential emitter materials but also play a crucial role as passive optical filters. This dual functionality is particularly relevant in increasing TPV efficiency. Another viable approach to enhance TPV efficiency is the use of wavelength-selective optical filters.[22] These filters work by reflecting photons below the bandgap while selectively transmitting photons above the bandgap into the TPV cell.^[2] The incorporation of a selective filter into a TPV system provides a benefit over not using any filter at all, in terms of spectral shaping and control of the emitter's spectral output. Reducing extremely high energy photons to a range just above the TPV cell bandgap energy may minimize thermalization losses and therefore improve cell conversion efficiency.^[2,23] Moreover, the temperature stability of material is of concern for selective emitters compared to selective filters that operate at lower temperatures. Selective filters also have an easier fabrication process than compared to selective cells making them the best choice for spectral control. A selective cell is a specialized type of photovoltaic device designed to efficiently convert thermal radiation, often in the form of infrared (IR) radiation, into electricity. The cells are engineered to operate in conjunction with a thermal emitter that provides the necessary thermal radiation. The distinguishing feature of these cells is their spectral selectivity, which means they selectively absorb and convert specific wavelengths of radiation while minimizing losses from nonabsorbed wavelengths.

Selective filters improve TPV systems through spectral control of incident radiant energy. A lot of research has been done on the selective optical filter using various mechanisms such as the interference effect and surface polariton resonance (SP) modes to achieve superior spectral performance of TPV systems. Rahmlow *et al.* demonstrated a 70 % spectrally efficient tandem filter coupled with 0.6 eV InGaAs cell that had high transmission below the bandgap due to a highly doped epitaxially grown layer of InPAs layer.^[24] A one dimensional (1D) 8-layer SiO₂/Si nanostructure TPV selective filter showed a 95% transmission at a wavelength of 1.73 μm

and reflected most of the radiated photons in the wavelength range from 1.73 to 3.9 μ m.^[25] A ten-layer quarter wave photonic crystal was designed and fabricated with 40% spectral efficiency for 1500 K blackbody emitter.^[4] A recent study suggested the use of a 1D photonic crystal with a passband range of 991 nm to 1788 nm as a filter for a GaSb cell with a bandgap of 0.7 eV.^[20]

Metasurfaces offer a versatile platform for tailoring the behavior of light, and ongoing research continues to expand their applications in various domains of science and technology. Their ability to manipulate light in precise and controllable ways makes them a fascinating area of study with a wide range of practical uses. They have emerged as a transformative technology with broad-ranging applications including cryptography, information storage and security tagging.[26] These two-dimensional arrays of subwavelength structures offer precise control over light-matter interactions. In the realm of optics, they enable remarkable advancements, polarization including control and measurement.[27] Additionally, metasurfaces have found utility in nonlinear, [28] exemplifying their versatility in tailoring optical responses.^[29] To gain a comprehensive understanding of metasurfaces and their potential, numerous review articles serve as valuable references.[30-32] In this research, we delve into the significance of metasurfaces in the development of advanced optical filters for Thermophotovoltaic (TPV) systems, highlighting their immense potential to enhance spectral control and system efficiency.

In this work, we numerically design a selective metasurface filter made of aluminum nanopillar (AlNP) array on a quartz substrate to achieve spectrally selective transmission above the bandgap of the TPV cell and theoretically analyze its effect on the TPV performance. Aluminum metal is preferred for the nanopillar structure due to its low cost, good stability and resistance to oxidation, ease of deposition and low infrared absorption properties.[26,33] Fullwave numerical simulations were performed to determine the appropriate nanopillar diameter, period, and height. An inductor-capacitor (LC) circuit model is used for verification of underlying physical mechanisms by comparison with numerical simulation. Furthermore, the incidence angle dependence on the transmission spectra and electromagnetic fields for elucidating the resonant transmission behavior of the nanopillar-based filter is investigated. By pairing the designed filter with a GaSb cell and a black emitter at 1000 K or higher, the TPV system performance is theoretically evaluated and compared to that without any filter and with ideal broadband and narrowband filters. Analysis of the TPV system indicates that the AINP metasurface selective filter, when combined with a GaSb cell, has the potential to achieve a higher TPV system efficiency compared to the case of a system using a black emitter without any filter. Further optimization of the metasurface filter could push TPV efficiency closer to the ideal limit of 38% set by a narrowband filter.

2. Theoretical Methods

2.1 Selective metasurface filter design and simulation method

The designed spectrally selective metasurface filter is made up of a vertically aligned subwavelength AlNP array coated on a quartz substrate as shown in Fig. 1(a). The nanopillar array period, diameter, and height are represented by the geometric parameters a, d, and h, respectively. The electric field and magnetic field directions of a transverse magnetic (TM or p-polarized) wave at normal incidence are also depicted in the image by \bar{E} and \bar{H} , respectively. Due to geometric symmetry, the optical response of the spectrally selective filter, such as spectral transmittance, will be the same under different polarized waves for normal incidence.

The finite-difference time-domain (FDTD) technique (Lumerical Solutions, Inc.) was used to acquire the radiative characteristics of the proposed selective metasurface filter over a wavelength range of 0.4 µm to 4 µm using 300 data points with mesh size of 5 nm. Wavelength-dependent material properties were obtained from Palik data for aluminum and quartz.[34] A plane-wave source with a 0° polarization angle (TM wave) was incident onto a unit cell of the periodic metasurface filter. Bloch boundary conditions were specified on both the y and z directions to account for phase changes between different periods, while perfectly matched layers were set on the x direction to eliminate wave reflections from simulation domain borders. By numerically solving Maxwell's equations, the reflection and transmission properties across the thin AINP layer can be obtained from the FDTD simulations. The FDTD validation and convergence check are provided in the Supporting Materials.

As the quartz substrate is thick and non-absorbing, ray-tracing optics^[35] was then used to calculate the reflectance and transmittance of the entire metasurface-on-quartz filter structure by incorporating those across the thin AlNP layer from the FDTD simulation as:

$$R_{filter} = \rho_{12} + \frac{\rho_s \tau^2 \tau_{12} \tau_{21}}{1 - \rho_s \rho_{21} \tau_{12} \tau_{21}} \tag{1}$$

$$\tau_{filter} = \frac{\tau_{12}\tau_{s}\tau}{1 - \rho_{s} \rho_{21}\tau_{12}\tau_{21}} \quad \& \quad T_{filter} = \left|\tau_{filter}\right|^{2} \quad (2)$$

where ρ_{12} or ρ_{23} refers to the reflectance of the nanopillar film structure for rays originating from air or the substrate; τ_{12} and τ_{21} are the corresponding transmittance as the wave propagation depicted in Fig. 1(b). Note that ρ_{12} , ρ_{23} , τ_{12} and τ_{21} were numerically obtained from FDTD at given wavelength, angle of incidence and polarization. ρ_s and τ_s represent the reflectance and transmittance for rays originating from the quartz substrate to the air and can be calculated using the Fresnel coefficients for a single interface. The internal transmittance τ of the substrate is:

$$\tau = exp\left(\frac{-4\pi k_s d_s}{\lambda \cos \theta_s}\right) \tag{3}$$

where k_s is the absorption coefficient of the substrate at the wavelength λ , d_s is the thickness of the substrate, and q_s is the refraction angle in the quartz substrate.

2.2 Theoretical modeling of TPV system with selective filters

A simple TPV system considered in this study consists of a black emitter, a spectrally selective optical filter and a GaSb cell as shown in Fig. 2(a). The GaSb cell has spectral absorptance $\alpha_c(\lambda)$ as shown in Fig. 2(b), where the cell has high absorptance near the bandgap of the cell (i.e., 1.9 μm).[1] The black emitter has unity emittance at all wavelengths as shown in Fig. 2(c). In this regard, the use of an optical filter becomes vital to improve the TPV system efficiency by transmitting only above-bandgap photons to the cell and reflecting below-bandgap photons for recycling. An ideal optical broadband filter transmits all the radiation above the bandgap of the TPV cell and reflects all the radiation below, where an ideal narrowband filter transmits photons within a narrow spectral range of λ_1 to λ_2 as shown in Fig. 2(d). The long cutoff wavelength λ_2 is fixed at 1.9 µm corresponding to the GaSb cell bandgap whereas the variable short cutoff wavelength λ_1 will be studied on how to impact the TPV system efficiency.

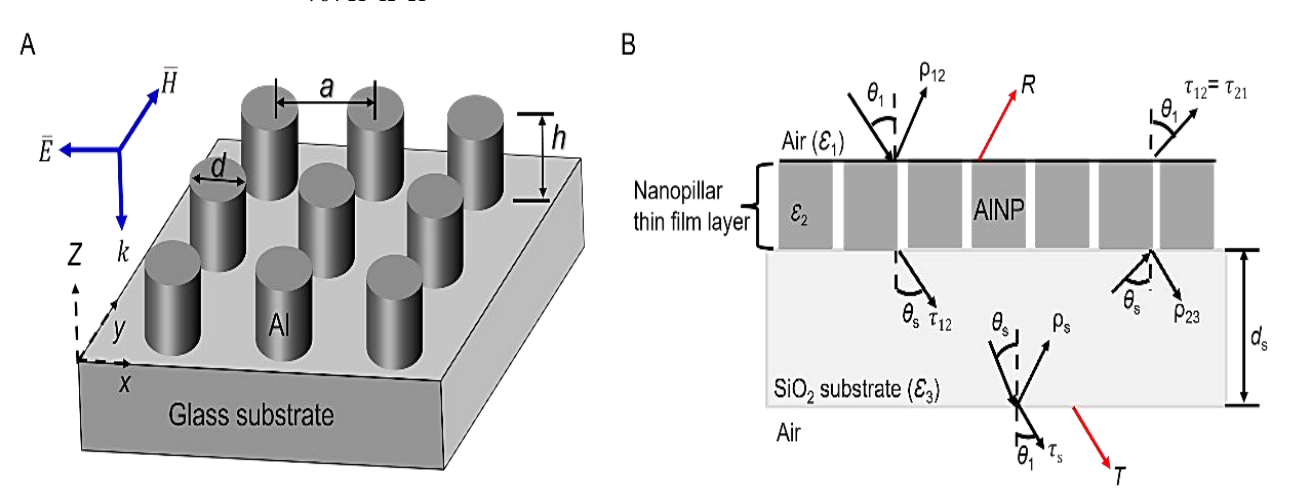


Fig. 1 (a) Three-dimensional schematic of the proposed aluminum nanopillar (AlNP) metasurface filter on quartz substrate with wave propagation at normal incidence. (b) Two-dimensional schematic of the proposed AlNP metasurface filter structure on a thick quartz substrate with the wave propagation at oblique angles of incidence.

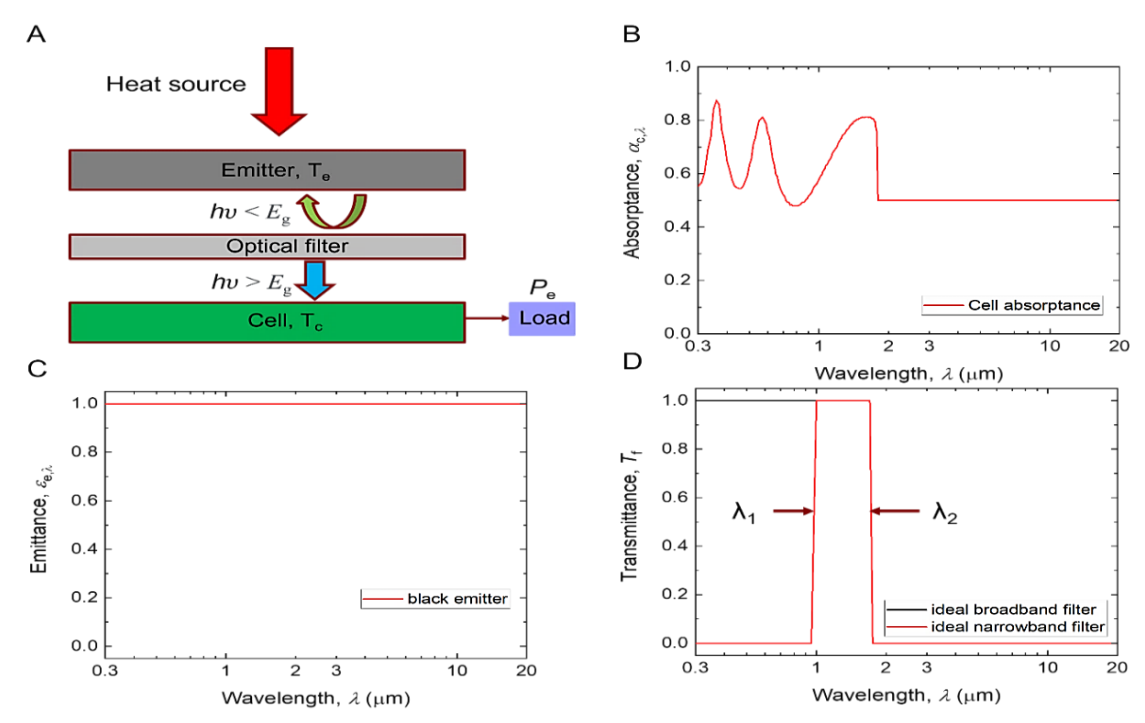


Fig. 2 (a) Schematic of a simple TPV system consisting of an emitter, an optical filter, and a cell, (b) spectral absorptance of the GaSb cell, (c) spectral emittance of a black emitter, and (d) spectral transmittance of an ideal broadband filter and a narrowband filter to transmit the light with energy above the bandgap of the GaSb cell (i.e., 1.9 µm).

a TPV system is defined as the ratio of the output electric power (P_e) to the total radiative heat flux incident (q_{in}) on the TPV cell:

$$\eta_{TPV} = \frac{P_e}{q_{in}} \tag{4}$$

The total incident radiative heat flux q_{in} on the TPV cell can be found from the spectral net radiative heat transfer between

the emitter and the cell across the filter
$$q_{e-c}(\lambda)$$
 as
$$q_{in} = \int_0^\infty q_{e-c}(\lambda) d\lambda = \int_0^\infty \frac{E_{b\lambda}(T_e) - E_{b\lambda}(T_c)}{\frac{1}{\epsilon_{\lambda e}} + \frac{1}{\epsilon_{\lambda c}} - 1}$$
(5)

where subscripts e and c represent emitter and cell, respectively. $\mathcal{E}_{\lambda,e} = 1$ for the black emitter and $\mathcal{E}_{\lambda,c} =$ $\tau_{filter}(\lambda)\alpha_c(\lambda)$ is the spectral emittance of the filtered cell, assuming that the optical filter absorbs negligible incoming radiation energy. The view factor between the emitter and the cell is assumed to be one here for simplicity and the emitter area and cell area are assumed to be equal. The emitter temperature $T_{\rm e}$ is varied from 1000 to 2000 K, while the filter and cell temperatures T_c are assumed to be 300 K. The blackbody emissive power $E_{b\lambda}(T)$ can be calculated by the Planck's law for a given temperature T.^[36]

Considering the current–voltage diode characteristics, the maximum generated power density $P_{\rm e}$ (W/cm²) is calculated

$$P_e = V_{OC} I_{SC} \left(1 - \frac{1}{X} \right) \left(1 - \frac{lnX}{X} \right) \text{ with } X = ln \left(\frac{I_{SC}}{I_0} \right)$$
 (6)

Note that I_{SC} is the short-circuit current density (A/cm²) calculated by:

$$I_{SC} = \int_{0}^{\frac{hc_0}{Eg}} \frac{e\lambda}{hc_0} \alpha_c(\lambda) \eta_i(\lambda) q_{e-c}(\lambda) d\lambda \tag{7}$$

The thermal-to-electricity energy conversion efficiency for where h is Planck's constant, c_0 is the speed of light in vacuum, e is the elementary electric charge, $E_{\rm g}$ is the bandgap of the GaSb cell (0.72 eV), $a_c(l)$ is the spectral absorptance of the GaSb cell, $\eta_i(\lambda)$ is the internal quantum efficiency (IQE) of the GaSb TPV cell from Ref. [38]. V_{OC} is the open-circuit voltage, which can be found by:[39]

$$V_{OC} = \left(\frac{k_B T_c}{e}\right) ln \left(\frac{I_{SC}}{I_0 + 1}\right)$$
 (8)

where $k_{\rm B}$ is the Boltzmann constant and $T_{\rm c}$ is the cell temperature (assumed to be 300 K). The dark current I_0 can be calculated by:[40]

$$I_0 = e \left(\frac{n_i^2 D_h}{L_h N_D} + \frac{n_i^2 D_e}{L_e N_A} \right)$$
 (9)

where n_i is the intrinsic carrier concentration of GaSb, N_D and $N_{\rm A}$ are respectively the donor concentration and acceptor concentration, D_h and D_e are respectively the hole diffusion coefficient and electron diffusion coefficient, and L_h and L_e are respectively the hole and electron diffusion length.[41] The values used for n_i , N_D , N_A , D_h , D_e , L_h and L_e and the validation of the TPV system calculation are provided in the Supporting Materials.

3. Results and Discussions

3.1 Spectral radiative properties

Figure 3 presents the calculated radiative properties of reflectance, transmittance and absorptance under normal incidence in the wavelengths from 0.4 to 10 µm for the proposed aluminum nanopillar metasurface filter on the 0.5mm-thick quartz substrate with base geometric values of pillar diameter d = 370 nm, period a = 450 nm, and height h = 700nm. Clearly, close to the GaSb cell bandgap around 1.9 mm, a

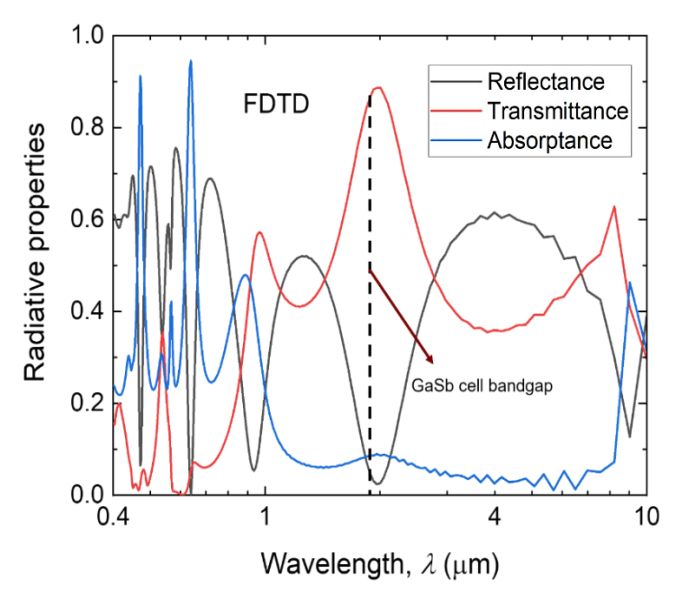


Fig. 3 Calculated spectral reflectance, transmittance, and absorptance of the selective AlNP metasurface filter on the 0.5-mm-thick quartz substrate at normal incidence with nanopillar diameter d = 370 nm, period a = 450 nm and heigh h = 700 nm.

major transmission peak with transmittance as high as 0.90 is observed, suggesting the desired filtering effect for the TPV cell. In addition, two minor transmittance peaks also occur around the wavelengths of 0.93 μ m and 0.54 μ m. Associated with the transmission peaks, suppressed reflection, and enhanced absorption can also be seen, indicating some

resonance behaviors inside the metasurface structure for the unusual optical responses.

3.2 Excitation of magnetic polariton

To elucidate the resonance effect indicated by the spectra, the electromagnetic field distributions at resonance wavelengths of 1.9 µm, 0.93 µm, and 0.54 µm are plotted using FDTD as shown in Figs. 4(b), (c) and (d). The electric field vectors are represented by arrows, and the magnetic field normalized to the incident field as seen from the contour plots. The confinement of the magnetic energy between the nanopillars can be clearly seen from the field plots, whereas the electric field pointing in opposite directions indicate that the electric field forms a closed loop surrounding the confining region (the circles between the pillars). Deep grating[42] and nanowirebased metamaterial absorbers or emitters[43,44] have shown similar behavior that has been proven to be the resonance of magnetic polariton (MP).[45] When incoming electromagnetic fields excite MP, an oscillating resonant electrical current is formed inside the nanopillar formations, which is caused by free charges at the surface. With severely restricted electromagnetic energy in the air gap, the resonant electrical current loop oscillates between nearby nanopillars, resulting in an increase in spectral transmittance at resonance wavelengths, as depicted by an inductor-capacitor (LC) circuit model in Fig. 4(a) for the fundamental MP mode. As shown in Figs. 4(c) and 4(d), higher harmonic modes of MP (i.e., MP2 and MP3) contribute to the selective transmittance

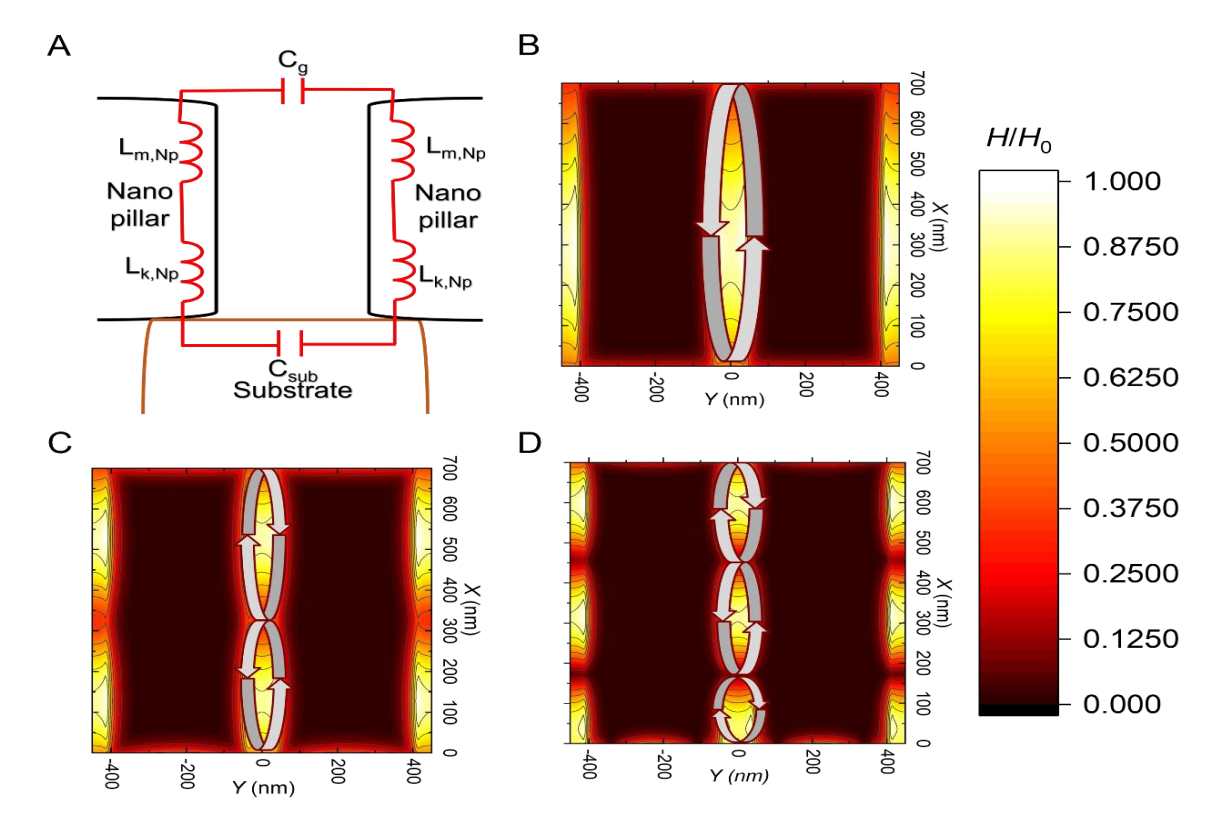


Fig. 4 (a) The LC circuit model based on charge distribution and contour plots of electromagnetic fields between the neighboring aluminum nanopillars when MP resonances are excited at wavelengths (b) 1.9 μ m, (c) 0.93 μ m, and (d) 0.54 μ m from FDTD simulations.

The harmonic modes play a significant role in the case of transmission spectra are investigated here. The spectral filters as they achieve high transmissions at wavelengths lower than the bandgap.

Analytical LC models based on surface charge distribution at MP resonant wavelength have been successfully applied to the resonance condition for grating-based metamaterials, as established in prior works.[46-48] For nanowire or nanopillar based structures, a modified LC model has been proposed by simplifying nanopillars to an effective plate, based on the similar strongly localized magnetic field distributions based on the literature.[43] The equivalent LC circuit model is used to predict the resonance for the fundamental mode. As shown in Fig. 4(a), C_g and C_{sub} forms a capacitor in the air gap and substrate respectively between the nanopillars, $L_{\rm m, NP}$ is the mutual inductance between the nanopillars, and $L_{k,NP}$ is the kinetic inductance contributed by the drifting electrons in the nanopillars. Therefore, the total impedance of the LC circuit can be expressed as:

$$Z_{total} = i\left[\omega\left(2L_{m,NP} + L_{k,NP}\right) - \frac{1}{\omega C_g} - \frac{1}{\omega C_{sub}}\right]$$
(10)

where.

where,
$$L_{m,NP} = 0.5\mu_0 hb$$

$$L_{k,NP} = \frac{b}{\varepsilon_0 \, \delta_{NP} \omega^2 \varepsilon_{NP}'}$$

$$C_{sub} = c_2 \varepsilon_0 \varepsilon_{sub} \frac{h}{b}$$

$$C_g = c_1 \varepsilon_0 \frac{h}{h}$$

where μ_0 is the magnetic permeability of free space, \mathcal{E}_0 is the permittivity of free space, \mathcal{E}_{sub} is the dielectric function (real part) of SiO_2 , h is the height of the nanopillar, and b is the difference between the interpore distance (a) and diameter of the nanopillars (d). The non-uniform charge distribution factor c_1 and c_2 of 0.2 to 0.3 is typical. [49] In this computation, to accommodate for the curved surface of the nanowire the nonuniform charge distribution factor c_1 is set as 0.4 based on prior literature^[43] and c_2 to be 0.1 due to negligible effect of the non-absorbing quartz substrate. MP resonance occurs when the overall impedance Z_{total} is zero, from which the MP resonance wavelength λ_0 can be calculated for the fundamental mode.

As a result, the LC circuit model predicts a resonance wavelength of 1.88 µm for MP1 for the AlNP metasurface filter with the base geometry (diameter d = 370 nm, period a = 450 nm, and height h = 700 nm), which agrees with the value (1.9 µm) found via FDTD simulation, confirming that the resonances and selective transmission are attributable to the excitation of magnetic polaritons at these selected wavelengths.

3.3 Geometric dependence

As indicated by the LC model, the geometric parameters of the AINP metasurface filter will affect the MP resonance and thus the transmission and absorption spectra. Therefore, the impact

at shorter resonance wavelengths around 0.93 µm and 0.54 µm. of those geometric parameters on the MP resonance and normal transmittance of the AINP metasurface filter structure was simulated by altering the nanopillar diameter (d), period (a), and height (h) separately while keeping other two geometric parameters fixed at the base values (i.e., d = 370 nm, a = 450 nm, and h = 700 nm). Fig. 5(a) demonstrates the influence of nanopillar height varying from 200 to 800 nm on spectral transmittance, where the major transmission peak red shifts to longer wavelengths significantly with longer nanopillars. With the AINP diameter increasing from 200 nm to 400 nm as shown in Fig. 5(b), the transmission peak redshifts slightly, which is consistent with prior observations about its impact on the MP resonance wavelength^[43] In particular, the transmission value increases with smaller diameters because there are larger gaps between nanopillars for the light to pass through as expected. Fig. 5(c) illustrates the spectral transmission with different array periods from 400 nm to 500 nm where the simulation result shows that the resonance peaks blue shift to shorter wavelengths with larger array period. Meanwhile, the amplitude of the transmission peaks at shorter wavelengths also increased slightly.

To better understand the geometric dependence, the MP1 resonance wavelengths obtained by FDTD simulation are compared with those predicted by the LC circuit model with varied geometric parameters. Fig. 5(e) depicts a comparison of the MP resonance wavelength as a function of nanopillar diameter between the FDTD simulations and the LC circuit model prediction. The MP resonance wavelength increases monotonically with nanopillar diameter, as anticipated by the LC circuit model, due to increase in capacitance and inductance values. Similar agreements are seen for the impacts of nanopillar height and period, as illustrated in Figs. 5(d) and 5(f), which further validate the MP resonance that is responsible for the selective transmission and predict the geometric dependence with the analytical LC model.

3.4 Effects of incidence angle and polarization

6 presents the simulated spectral-directional transmittance of the AlNP metasurface TPV filter at multiple oblique incidence angles (i.e., 0° , 15° , 30° , 45° , 60°) under TM and TE polarized waves in the wavelength range from 0.4 to 2 μm, within which the three transmission peaks associated with MP resonances observed previously under normal incidence exist. As shown in Fig. 6, these three resonance transmission peaks exhibit minor change with incidence angles up to 60° for both TM and TE waves, indicating angle and polarization insensitivity, which is a unique characteristics of MP resonance as seen in prior literature.[43] In particular, the spectral transmittance of the AlNP metasurface filter is still approximately 0.8 at 60° incidence for both polarizations around 1.9 mm wavelength, which is the GaSb cell bandgap. This diffuse behavior and polarization independence is beneficial for the proposed metasurface filter to maintain its high wavelength selectivity right above the cell bandgap even

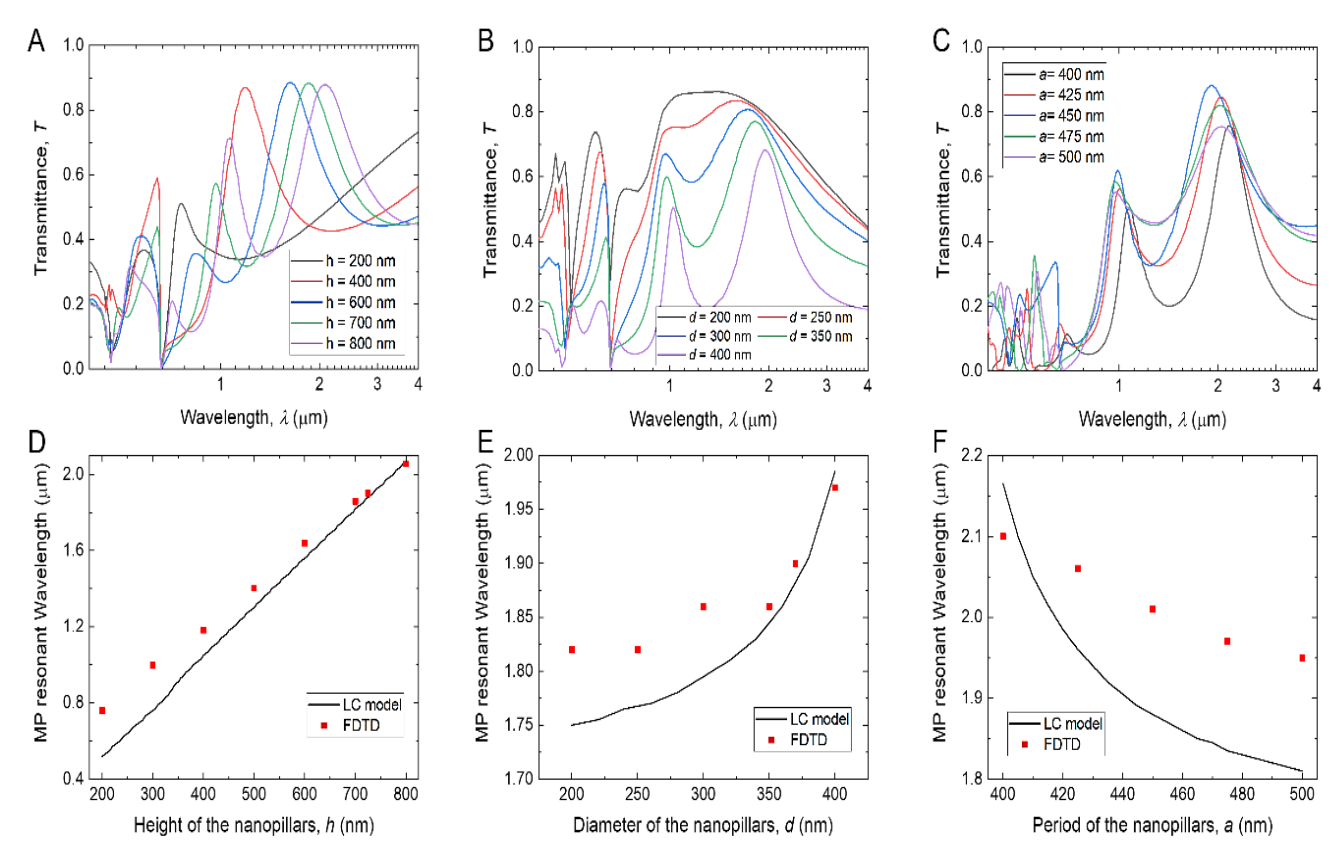


Fig. 5 The simulated spectral transmittance with respect to one varying geometric parameter of aluminum nanopillars: (a) diameter, (b) height and (c) period. The MP1 resonance wavelengths predicted by FDTD and by the LC circuit model with respect to one varying geometric parameter of nanopillars: (d) diameter, (e) height and (f) period. The base geometric values are d = 370, a = 450 nm, and b = 700 nm.

at large oblique angles, which in turn would help improve the TPV performance.

3.5 Theoretical prediction of TPV system performance with selective filters

To evaluate how the proposed AlNP metasurface filter would impact the TPV system performance, the spectral efficiency is

quantitatively calculated as shown in Fig. 7(a) for the proposed AlNP metasurface selective filter selective filter coupled with a black emitter ($\varepsilon_{e,\lambda} = 1$) at different temperatures. The spectral efficiency is defined as the percentage of photons absorbed by the PV cell from the emitter. For comparison, the spectral efficiencies without any filter and with ideal narrowband with short cutoff wavelength at 1 µm and

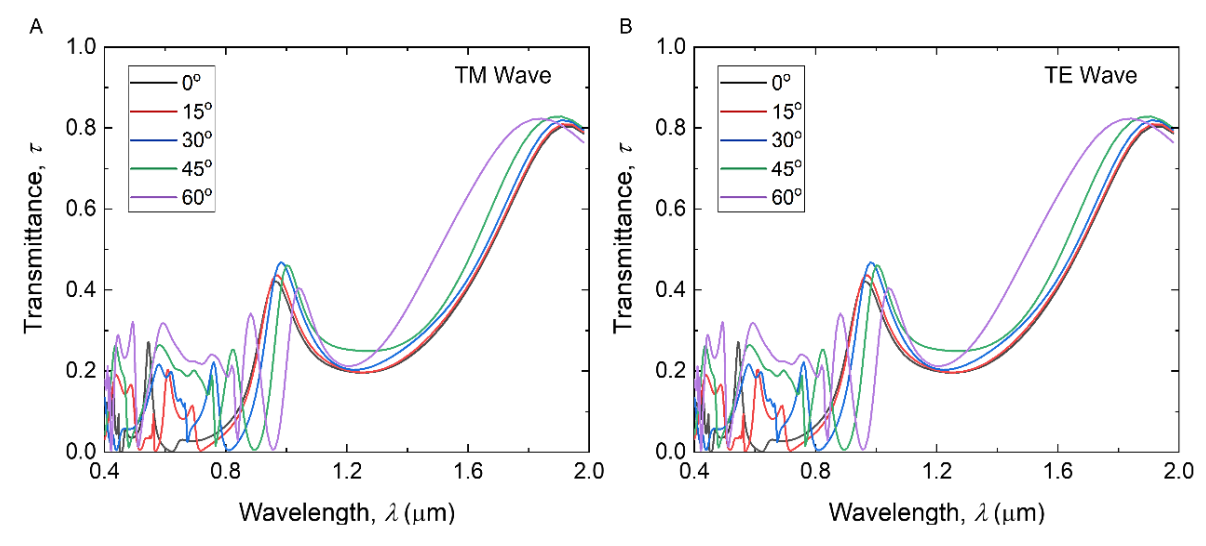


Fig. 6 Simulated spectral-directional transmittance of the proposed AlNP metasurface filter at multiple incidence angles for (a) TM waves and (b) TE waves.

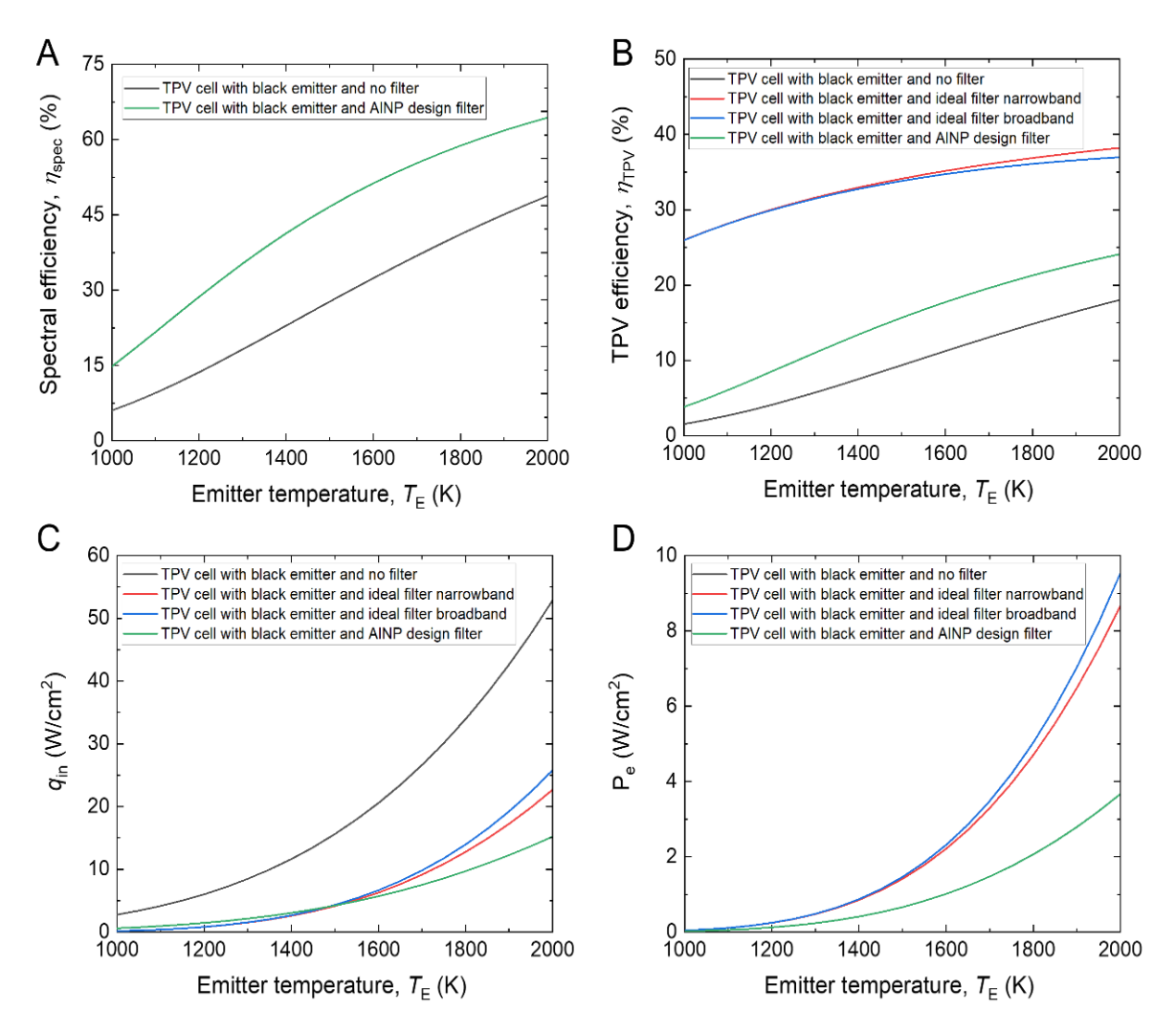


Fig. 7 (a) Spectral efficiency, (b) TPV efficiency, (c) net radiative heat flux and (d) output power at different blackbody emitter temperatures from 1000 K to 2000 K without any filter, with designed AlNP metasurface selective filter, and ideal broadband and narrowband filters when paired with a GaSb cell. The power produced by the TPV cell with black emitter and no filter is overlaid by curve of TPV cell with black emitter and ideal broadband filter as they have the same values in (d).

broadband filters coupled with the black emitter are also shown. The spectral efficiency improves with emitter temperature because the thermal radiation spectrum moves to a lower wavelength as temperature rises, increasing the fraction of photons with energies above the cell's bandgap. The proposed AlNP metasurface filter improves the spectral efficiency to 15% at 1000 K from 5% for the standalone black emitter, and to 65% at 2000 K from 49% for the standalone black emitter. For the ideal narrowband and broadband filters, the spectral efficiencies are 100% for all emitter temperatures.

Figures 7(b)–(d) show the predicted TPV efficiency η_{TPV} , net radiative heat flux q_{in} between the black emitter and the GaSb cell through the filter, and the output power P_e from the GaSb cell, respectively for the cases without any filter, with the designed AlNP metasurface selective filter, and with ideal broadband and narrowband filters. The TPV system efficiency ranges from 1.5% to 18% for the standalone black emitter without any filter at emitter temperatures from 1000 to 2000 K. With the designed AlNP metasurface filter, the TPV

efficiency improves to 3.8% at 1000 K and to 24.1% at 2000 K because of the spectral selectivity of the designed filter with lower transmission below the bandgap. For an ideal GaSb cell with 100% IQE and the designed metasurface filter, the TPV efficiency can be further improved up to 31.1% at 2000 K as shown in Fig. S7. For the ideal filters, both the broadband and narrowband ones could achieve TPV efficiency of 25.5% at 1000 K and around 37.5% at 2000 K as shown in Fig. 7(b) due to the perfect spectral filtering of below-bandgap unusable photons. Note that the ideal narrowband filter outperforms the broadband one at 2000 K by ~1.5% more TPV efficiency, which could be understood by the excessive high-energy photons' way above the cell bandgap through the ideal broadband filter.

Figures 7(c) and 7(d) respectively plot the net radiative heat flux incident on the cell $q_{\rm in}$ and the cell power output $P_{\rm e}$ as a function of the black emitter temperature. With the designed AlNP metasurface filter, the net radiative heat flux is about the same as that with either broadband or narrowband

ideal filter up to 1500 K, while the power generated with ideal filters exceed that with the metasurface filter as emitter temperature increases. This could be understood by more useful photos are available at higher temperature above the cell bandgap and ideal filters reflect all the below-bandgap photons back to the emitter for recycling. After all, only photons with energy exceeding the cell bandgap could be converted into electrical power by the cell. On the other hand, the TPV system without any filter has the highest net radiative heat flux but produces the same amount of power as the system with the ideal broadband filter, leading to the lowest TPV efficiency due to the black emitter without spectral selectivity. In particular at the emitter temperature of 2000 K, the TPV system with the designed AlNP metasurface filter could generate power $P_e = 3.67 \text{ W/cm}^2$, which could be possibly further improved approaching 9.5 W/cm² set by the ideal broadband filter.

It should be noted that the analysis above is based on the in-band spectral absorptance of the GaSb cell acquired from Ref. [38] and the out-of-band absorptance assumed to be 0.5 as a nominal value from typical GaSb cells by JX Crystals. [50–52] It is known that the below-bandgap cell absorptance could significantly affect the TPV performance, and the lower cell absorption below the bandgap would enhance the TPV efficiency. Please see the calculation results for below-bandgap absorptance of the GaSb cell using nominal values of 0.05, 0.2, 0.75 and 0.95 on the TPV system efficiency, spectral efficiency, net radiative flux, and output power in the Supporting Materials.

4. Conclusions

In summary, this work has theoretically studied an aluminum nanopillar metasurface filter as a narrowband filter for enhancing TPV system performance. The radiative characteristics of the selective metasurface filter were simulated using FDTD modeling, and the excitation of MP modes between the nanopillars were identified to result in the selective transmissions above the GaSb cell bandgap. LC circuit model and the electromagnetic field distribution were used to clarify the underlying physical mechanism. The effects of geometric parameters, incidence angles and polarizations were studied systematically on the selective transmission spectra of the metasurface filter. The theoretical TPV system analysis suggests the designed AlNP metasurface selective filter combined with a GaSb cell could achieve a TPV efficiency of 24.1% and an output power of 3.67 W/cm² at the black emitter temperature of 2000 K. With further optimization of the metasurface filter, the TPV efficiency could be improved approaching 38% set by the ideal narrowband filter. This study will facilitate the research and development of metasurface based spectrally selective filters for high-efficiency TPV devices. This study could be further extended by fabricating metasurface through the utilization of anodized aluminum oxide (AAO) templates. [53-55] AAO templates are known for their ability to fabricate periodic

nanostructures efficiently and at a lower cost.^[55] The proposed filter design could be fabricated in a 3-step process; Firstly, AAO membrane transference on quartz wafer, followed by ebeam deposition of aluminum on AAO templatized quartz and finally AAO template removal.

Acknowledgement

This work was supported by the Air Force Office of Scientific Research under Grant No. FA9550-17-1-0080.

Conflict of Interest

There is no conflict of interest.

Supporting Information

Applicable.

References

- [1] M. M. Ali Gamel, H. J. Lee, Wan Emilin Suliza Wan Abdul Rashid, P. J. Ker, L. K. Yau, M. A. Hannan, M. Z. Jamaludin, A review on thermophotovoltaic cell and its applications in energy conversion: issues and recommendations, *Materials*, 2021, **14**, 4944, doi: 10.3390/ma14174944.
- [2] C. Ferrari, F. Melino, M. Pinelli, P. R. Spina, M. Venturini, Overview and status of thermophotovoltaic systems, *Energy Procedia*, 2014, **45**, 160-169, doi: 10.1016/j.egypro.2014.01.018. [3] L. P. Wang, Z. M. Zhang, Wavelength-selective and diffuse emitter enhanced by magnetic polaritons for thermophotovoltaics, *Applied Physics Letters*, 2012, **100**, 2010–2013, doi: 10.1063/1.3684874.
- [4] L. Mao, H. Ye, New development of one-dimensional Si/SiO₂ photonic crystals filter for thermophotovoltaic applications, *Renewable Energy*, 2010, **35**, 249-256, doi: 10.1016/j.renene.2009.06.013.
- [5] J. Li, F. Zhao, W.-C. Shih, Direct-write patterning of nanoporous gold microstructures by *in situ* laser-assisted dealloying, *Optics Express*, 2016, **24**, 23610, doi: 10.1364/oe.24.023610.
- [6] S. Basu, Y.-B. Chen, Z. M. Zhang, Microscale radiation in thermophotovoltaic devices—a review, *International Journal of Energy Research*, 2007, **31**, 689-716, doi: 10.1002/er.1286.
- [7] D. Wilt, D. Chubb, D. Wolford, P. Magari, C. Crowley, Thermophotovoltaics for Space Power Applications, AIP Conference Proceedings. Madrid (Spain). AIP, 2007, **890**, 335-345, doi: 10.1063/1.2711751.
- [8] L. Fraas, R. Ballantyne, J. Samaras, M. Seal, Electric power production using new GaSb photovoltaic cells with extended infrared responseAIP Conference Proceedings. Copper Mountain, Colorado (USA). AIP, 1995, 44, 44-53, doi: 10.1063/1.47053.
- [9] A. Datas, A. Ramos, A. Martí, C. del Cañizo, A. Luque, Ultra high temperature latent heat energy storage and thermophotovoltaic energy conversion, *Energy*, 2016, **107**, 542-549, doi: 10.1016/j.energy.2016.04.048.
- [10] T. Bauer, I. Forbes, N. Pearsall, The potential of thermophotovoltaic heat recovery for the UK industry, *International Journal of Ambient Energy*, 2004, **25**, 19-25, doi:

10.1080/01430750.2004.9674933.

- [11] Y. Xuan, X. Chen, Y. Han, Design and analysis of solar thermophotovoltaic systems, *Renewable Energy*, 2011, **36**, 374-387, doi: 10.1016/j.renene.2010.06.050.
- [12] W. R. Chan, V. Stelmakh, C. M. Waits, M. Soljacic, J. D. Joannopoulos, I. Celanovic, Photonic crystal enabled thermophotovoltaics for a portable microgenerator, *Journal of Physics: Conference Series*, 2015, **660**, 012069, doi: 10.1088/1742-6596/660/1/012069.
- [13] T. Burger, C. Sempere, B. Roy-Layinde, A. Lenert, Present efficiencies and future opportunities in thermophotovoltaics, *Joule*, 2020, **4**, 1660-1680, doi: 10.1016/j.joule.2020.06.021.
- [14] L. M. Fraas, Economic potential for thermophotovoltaic electric power generation in the steel industry. 2014 IEEE 40th Photovoltaic Specialist Conference (PVSC). June 8-13, 2014, Denver, CO, USA. IEEE, 2014, 766-770, doi: 10.1109/PVSC.2014.6925031.
- [15] M. Tan, L. Ji, Y. Wu, P. Dai, Q. Wang, K. Li, T. Yu, Y. Yu, S. Lu, H. Yang, Investigation of InGaAs thermophotovoltaic cells under blackbody radiation, *Applied Physics Express*, 2014, 7, 096601, doi: 10.7567/apex.7.096601.
- [16] T. C. Narayan, L. Y. Kuritzky, D. P. Nizamian, B. A. Johnson, E. J. Tervo, A. R. Young, C. Luciano, M. K. Arulanandam, B. M. Kayes, E. E. Perl, M. Limpinsel, P. Santhanam, J. Slack, W. Olavarria, J. Carapella, M. Young, C-L. Wu, Z. J. Yu, Z. C. Holman, R. R. King, M. A. Steiner, D. M. Bierman, A. J. Ponec, J. A. Briggs, World record demonstration of > 30% thermophotovoltaic conversion efficiency, Conference Record of the IEEE Photovoltaic Specialists Conference, 2020, 1906, 1792-1795, doi: 10.1109/PVSC45281.2020.9300768.
- [17] A. LaPotin, K. L. Schulte, M. A. Steiner, K. Buznitsky, C. C. Kelsall, D. J. Friedman, E. J. Tervo, R. M. France, M. R. Young, A. Rohskopf, S. Verma, E. N. Wang, A. Henry, Thermophotovoltaic efficiency of 40%, *Nature*, 2022, **604**, 287-291, doi: 10.1038/s41586-022-04473-y.
- [18] Z. Utlu, B. S. Önal, Thermodynamic analysis of thermophotovoltaic systems used in waste heat recovery systems: an application, *International Journal of Low-Carbon Technologies*, 2018, **13**, 52-60, doi: 10.1093/ijlct/ctx019.
- [19] Fathi, Bendelala, Enhanced low-gap thermophotovoltaic cell efficiency for a wide temperature range based on a selective metamaterial emitter, *Solar Energy*, 2018, **174**, 1053-1057, doi: 10.1016/j.solener.2018.10.006.
- [20] S. Chakraborty, R. Ghosh, A. Chatterjee, A high temperature optical filter using Si/Si_3N_4 one dimensional photonic crystal for GaSb thermophotovoltaic applications, *American Journal of Electronics & Communication*, 2021, **2**, 19-22, doi: 10.15864/ajec.2205.
- [21] G. Mirbagheri, D. T. Crouse, Design, fabrication, and spectral characterization of TM-polarized metamaterials-based narrowband infrared filter, Terahertz, RF, Millimeter, and Submillimeter-Wave Technology and Applications XV. January SPIE, 2022, **12000**, 96-108, doi: 10.1117/12.2626405.
- [22] A. Pirvaram, N. Talebzadeh, M. Rostami, S. N. Leung, P. G. O'Brien, Evaluation of a ZrO₂/ZrO₂-aerogel one-dimensional

photonic crystal as an optical filter for thermophotovoltaic applications, *Thermal Science and Engineering Progress*, 2021, **25**, 100968, doi: 10.1016/j.tsep.2021.100968.

- [23] D. L. Chubb, B. S. Good, A combined thermophotovoltaic-thermoelectric energy converter, *Solar Energy*, 2018, **159**, 760-767, doi: 10.1016/j.solener.2017.11.030.
- [24] T. R. Jr, J. Lazo-Wasem, and E. Gratrix, Front Surface Tandem Filters using Sapphire (Al₂O₃) Substrates for Spectral Control in Thermophotovoltaic Energy Conversion Systems, 2005.
- [25] S. G. Babiker, Y. Shuai, M. O. Sid-Ahmed, M. Xie, Design of a one—Dimensional Si/SiO₂ photonic crystals filter for thermophotovoltaic application. INMIC. December 19-20, 2013, Lahore, Pakistan. IEEE, 2014, 177-181, doi: 10.1109/INMIC.2013.6731346.
- [26] S. J. Tan, L. Zhang, D. Zhu, X. M. Goh, Y. M. Wang, K. Kumar, C.-W. Qiu, J. K. W. Yang, Plasmonic color palettes for photorealistic printing with aluminum nanostructures, *Nano Letters*, 2014, **14**, 4023-4029, doi: 10.1021/nl501460x.
- [27] P. C. Wu, W.-Y. Tsai, W. T. Chen, Y.-W. Huang, T.-Y. Chen, J.-W. Chen, C. Y. Liao, C. H. Chu, G. Sun, D. P. Tsai, Versatile polarization generation with an aluminum plasmonic metasurface, *Nano Letters*, 2017, 17, 445-452, doi: 10.1021/acs.nanolett.6b04446.
- [28] M. Semmlinger, M. L. Tseng, J. Yang, M. Zhang, C. Zhang, W.-Y. Tsai, D. P. Tsai, P. Nordlander, N. J. Halas, Vacuum ultraviolet light-generating metasurface, *Nano Letters*, 2018, **18**, 5738-5743, doi: 10.1021/acs.nanolett.8b02346.
- [29] W. Yue, S. Gao, S.-S. Lee, E.-S. Kim, D.-Y. Choi, Highly reflective subtractive color filters capitalizing on a silicon metasurface integrated with nanostructured aluminum mirrors, *Laser & Photonics Reviews*, 2017, **11**, 1600285, doi: 10.1002/lpor.201600285.
- [30] H.-H. Hsiao, C. H. Chu, D. P. Tsai, Metasurfaces: fundamentals and applications of metasurfaces (small methods 4/2017), *Small Methods*, 2017, **1**, 1600064, doi: 10.1002/smtd.201770041.
- [31] M. K. Chen, X. Liu, Y. Sun, D. P. Tsai, Artificial intelligence in meta-optics, *Chemical Reviews*, 2022, **122**, 15356-15413, doi: 10.1021/acs.chemrev.2c00012.
- [32] M. K. Chen, Y. Wu, L. Feng, Q. Fan, M. Lu, T. Xu, D. P. Tsai, Principles, functions, and applications of optical meta-lens (advanced optical materials 4/2021), *Advanced Optical Materials*, 2021, 9, 2170013, doi: 10.1002/adom.202170013.
- [33] V. Liberman, K. Diest, C. W. Stull, M. T. Cook, D. M. Lennon, M. Rothschild, S. Schoeche, Wafer-scale aluminum nanoplasmonic resonators with optimized metal deposition, *ACS Photonics*, 2016, **3**, 796-805, doi: 10.1021/acsphotonics.5b00751. [34] E. D. Palik, Handbook of Optical Constants of Solids. Academic Press, 1998. doi: 10.1016/B978-012544415-6.50002-0
- [35] C. L. Mitsas, D. I. Siapkas, Generalized matrix method for analysis of coherent and incoherent reflectance and transmittance of multilayer structures with rough surfaces, interfaces, and finite substrates, *Applied Optics*, 1995, 34, 1678-1683, doi:

10.1364/AO.34.001678.

[36] T. L. Bergman, T. L. Bergman, F. P. Incropera, D. P. Dewitt, and A. S. Lavine, Fundamentals of heat and mass transfer. John Wiley & Sons, 2011.

- [37] K. Park, W. P. King, Performance analysis of near-field devices considering thermophotovoltaic absorption distributionProceeding of the 5th International Symposium on Radiative Transfer. Bodrum, Turkey. Connecticut: Begellhouse, 2007, doi: 10.1615/ichmt.2007.radtransfproc.270.
- [38] L. Tang, H. Ye, and J. Xu, A novel zinc diffusion process for the fabrication of high-performance GaSb thermophotovoltaic cells, Solar Energy Materials and Solar Cells, 2014, 122, 94-98, doi: 10.1016/j.solmat.2013.11.027.
- [39] K. Park, S. Basu, W. P. King, Z. M. Zhang, Performance analysis of near-field thermophotovoltaic devices considering absorption distribution, Journal of Quantitative Spectroscopy and Radiative 2008. 109. 305-316, Transfer, doi: 10.1016/j.jqsrt.2007.08.022.
- [40] Q. Ni, R. Ramesh, C.-A. Chen, L. Wang, Semiconductorbased selective emitter with a sharp cutoff for thermophotovoltaic energy conversion, Optics Letters, 2021, 46, 3163-3166, doi: 10.1364/OL.428215.
- [41] J. K. Tong, W.-C. Hsu, Y. Huang, S. V. Boriskina, G. Chen, Thin-film 'thermal well' emitters and absorbers for highefficiency thermophotovoltaics, Scientific Reports, 2015, 5, 10661, doi: 10.1038/srep10661.
- [42] B. Zhao, Z. M. Zhang, Study of magnetic polaritons in deep gratings for thermal emission control, Journal of Quantitative Spectroscopy and Radiative Transfer, 2014, 135, 81-89, doi: 10.1016/j.jqsrt.2013.11.016.
- [43] J.-Y. Chang, H. Wang, L. Wang, Tungsten nanowire metamaterials as selective solar thermal absorbers by excitation of magnetic polaritons, Journal of Heat Transfer, 2017, 139, 052401, doi: 10.1115/1.4034845.
- [44] H. Alshehri, S. Taylor, S. Liu, Y. Liu, R. Wang, L. Wang, Selective color metamaterial absorber made of aluminum nanodisk arrays by excitation of magnetic polaritons, ES Materials de *Manufacturing*, 2022, 17, 63-72, 10.30919/esmm5f630.
- [45] Q. Ni, H. Alshehri, L. Wang, Highly efficient sub-100-nm thermophotovoltaic cells enhanced by spectrally selective twodimensional metasurface, *Journal of Photonics for Energy*, 2018, 9, 032704, doi: 10.1117/1.JPE.9.032704.
- [46] L. P. Wang, Z. M. Zhang, Measurement of coherent thermal emission due to magnetic polaritons in subwavelength microstructures, Journal of Heat Transfer, 2013, 135, 091505, doi: 10.1115/1.4024469.
- [47] C.-J. Chen, J.-S. Chen, Y.-B. Chen, Optical responses from lossy metallic slit arrays under the excitation of a magnetic polariton, *Josa B*, 2011, **28**, 1798-1806, doi: C.-J. Chen, J.-S. Chen, Y.-B. Chen, Optical responses from lossy metallic slit arrays under the excitation of a magnetic polariton, Josa B, 2011, 28, 1798-1806.
- based on a large-area metasurface, Optical Materials Express, University of Science and Technology of China since 2021.

2017, 7, 618, doi: 10.1364/ome.7.000618.

- [49] Q. Ni, H. Alshehri, Y. Yang, H. Ye, L. Wang, Plasmonic light trapping for enhanced light absorption in film-coupled ultrathin metamaterial thermophotovoltaic cells, Frontiers in Energy, 2018, 12, 185-194, doi: 10.1007/s11708-018-0522-x.
- [50] Rajendra, Bhatt, High-efficiency solar thermophotovoltaic system using a nanostructure-based selective emitter, Solar *Energy*, 2020, **197**, 538-545, doi: 10.1016/j.solener.2020.01.029. [51] R. Bhatt, M. Gupta, Design and validation of a highefficiency planar solar thermophotovoltaic system using a spectrally selective emitter, *Optics Express*, 2020, **28**, 21869, doi: 10.1364/oe.394321.
- [52] A. Kohiyama, M. Shimizu, K. Konno, T. Furuhashi, H. Yugami, Effective photon recycling in solar thermophotovoltaics using a confined cuboid emitter, Optics Express, 2020, 28, 38567, doi: 10.1364/oe.412764.
- [53] C. Wang, Y. Wen, J. Sun, J. Zhou, Recent progress on optical frequency conversion in nonlinear metasurfaces and nanophotonics, ES Materials & Manufacturing, 2022, 17, 1-13, doi: 10.30919/esmm5f655.
- [54] G. Meng, T. Yanagida, K. Nagashima, T. Yanagishita, M. Kanai, K. Oka, A. Klamchuen, S. Rahong, M. Horprathum, B. Xu, F. Zhuge, Y. He, H. Masuda, T. Kawai, Facile and scalable patterning of sublithographic scale uniform nanowires by ultrathin AAO free-standing membrane, RSC Advances, 2012, 2, 10618, doi: 10.1039/c2ra21643d.
- [55] C. Yang, W. Mu, C. Ji, Z. Wang, H. Yuan, K. Li, X. Zheng, Y. Zhang, W. Shen, Optical device based on a nanopillar array by the pattern transfer of an anodic aluminum oxide membrane, ACS Applied Materials & Interfaces, 2019, 11, 36817-36823, doi: 10.1021/acsami.9b10338.

Author Information



Rajagopalan Ramesh received his Ph.D. in Aerospace Engineering from Arizona State University in 2022. His thesis is concentrated on the Study of Optical and Radiative Properties of Inhomogeneous Metallic Structures. During his PhD study, he has published

three first-authored journal papers, in addition to another 2 co-authored journal publications. The author is currently working as an optical engineer at Meta.



Qing Ni received her Ph.D. in engineering thermophysics at the University of Science and Technology of China in 2017 with Dr. Hong Ye. She was a postdoctoral research associate in Dr. Liping Wang's group at Arizona State University from 2017 to 2020. Currently, she is an associate research

[48] Y. Matsuno, A. Sakurai, Perfect infrared absorber and emitter professor in thermal science and energy engineering at the

Her research interests include radiation control in energy conversion, supercritical CO2 phase change theory and application.



Hassan Alshehri is an assistant professor in the Mechanical Engineering Department at King Saudi University (Saudi Arabia). He received his Ph.D. in Mechanical Engineering from Arizona State University (USA) in 2018. His main research interests include solar energy

harvesting, nanoscale radiative heat transfer, and tuneable selective metamaterials.



Bruno Azeredo received his Ph.D. degree from the University of Illinois at Urbana-Champaign in 2016. He joined as an assistant professor in 2017 at Arizona State University and became an associate professor from 2023 till now. His main research interests include scalable

nanomaterial synthesis and its size-dependent properties with an eye on exploiting them in additive- and nanomanufacturing platforms and enabling the production of multi-scale and multi-material structures.



Liping Wang received his Ph.D. degree from Georgia Institute of Technology in 2011. He joined as an assistant professor in 2012 at Arizona State University and became an associate professor from 2018 till now. His main research interests include metamaterials and nanoscale thermal

radiation for thermophotonic energy conversion and radiative thermal control.

Publisher's Note: Engineered Science Publisher remains neutral with regard to jurisdictional claims in published maps and institutional affiliations.